Novel On-Resistance based Methodology for MOSFET Electrical Characterization

T.A. Karatsori, K. Bennamane, Gérard Ghibaudo

Novel On-Resistance based Methodology for MOSFET Electrical Characterization

T. A. Karatsori[1], K. Bennamane[2], G. Ghibaudo[1]

1) IMEP-LAHC, Univ. Grenoble Alpes, Minatec, 38016 Grenoble, France.

2) University of M. Mammeri, Tizi-Ouzou, Algeria.

e-mail address: theano.karatsori@grenoble-inp.fr, ghibaudo@minatec.inpg.fr

Abstract

A new methodology for MOSFET characterization making use of the on-resistance characteristics $R_{on}(V_g,V_d)=V_d/I_d(V_g,V_d)$ and associated derivatives dR_{on}/dV_g and dR_{on}/dV_d is proposed. This approach enables to eliminate the influence of source-drain series resistance R_{sd} not only in linear region but also in non-linear region of MOSFET operation. Therefore, it allows for intrinsic MOSFET parameter extraction free from source and drain series resistance.

Keywords: MOSFET, parameter extraction, On-resistance.

1. Introduction

A precise extraction of MOSFET electrical parameters is needed for the proper engineering and optimization of CMOS technologies. Numerous methods have been proposed during the past decades for the MOSFET parameter extraction, mainly based on the $I_d(V_g,V_d)$ transfer or output drain current characteristics [1-12]. In this context, the Y-function technique, where $Y_g=I_d/\sqrt{g_m}$, g_m being the transconductance, has proven very efficient for MOSFET parameter extraction in linear region, since it eliminates the impact of source-drain series resistance R_{sd} [2, 7, 11, 12], at least when R_{sd} is constant with gate voltage.

In this paper, we propose a new methodology for MOSFET characterization making use of the on-resistance characteristics $R_{on}(V_g,V_d)=V_d/I_d(V_g,V_d)$ and associated derivatives dR_{on}/dV_g and dR_{on}/dV_d. Indeed, this approach enables to eliminate the influence of R_{sd} not only in linear region but also in non-linear region of MOSFET operation.

2. R_{on} Methodology principles

Considering Ohm's law, the power dissipated in a MOSFET, $P=I_dV_d$, can be expressed as [13],

$$P = I_d V_d = R_s I_d^2 + R_d I_d^2 + R_{on}^0 I_d^2 \tag{1}$$

where R_{on}^0 is the intrinsic on-resistance, R_s and R_d are the source and drain series resistances, respectively. Therefore, it can be shown from (1) that the extrinsic on-resistance R_{on} is simply obtained by adding R_s and R_d to the intrinsic on-resistance, R_{on}^0 as [13],

$$R_{on} = R_s + R_d + R_{on}^0 \tag{2}$$

As a result, Eq. (2) indicates that, as it was the case for MOSFET linear operation region [1-12], the use of on-resistance R_{on} allows generalizing the application of Ohm's law to the MOSFET non linear operation region. In turn, assuming as usual constant R_s and R_d, it implies that one could suppress the influence of the source and drain series resistance by dealing with its derivatives with

respect to V_g, as it was previously done in ohmic linear regime [1-12], but also with respect to V_d for any V_g and V_d bias condition.

It should be mentioned that this approach can be regarded as an attempt to generalize the concept of Y-function, originally derived for linear regime, to the non-linear operation region. Indeed, generalized Y-functions can be defined from the derivative of R_{on} with respect to V_g and V_d as:

$$Y_g = \sqrt{\frac{-V_d}{dR_{on}/dV_g}} \tag{3}$$

$$Y_d = \sqrt{\frac{V_d}{dR_{on}/dV_d}}\,. \tag{4}$$

It is worth noting that Eq. (3) naturally reduces to the standard definition for the Y-function, $Y_g=I_d/\sqrt{g_m}=\sqrt{\beta}.\sqrt{V_d}.(V_g-V_t)$ for small V_d at strong inversion.

A. *Long channel MOSFET at strong inversion*

For long channel devices, based on the classical MOSFET model valid in strong inversion, we have [14]:

$$I_d{}^L = \beta.V_d\,(V_{gt} - V_d/2) \quad \text{with} \quad \beta = \frac{W}{L}.C_{ox}.\mu_0 \tag{5}$$

where $V_{gt}=V_g-V_t$ is the gate voltage overdrive, C_{ox} the gate oxide capacitance per unit area, L the channel length, W the channel width and μ_0 the low-field mobility. It is easy to show using the definition of the total resistance ($R_{on}= V_d/I_d$) that the corresponding expressions for the on-resistance R_{on} and associated derivatives dR_{on}/dV_g and dR_{on}/dV_d are given by:

$$R_{on}{}^L = \frac{1}{\beta.(V_{gt} - V_d/2)} \tag{6}$$

$$\frac{dR_{on}{}^L}{dV_g} = \frac{-1}{\beta.(V_{gt} - V_d/2)^2} = -\beta.R_{on}^{L\,2} \tag{7}$$

$$\frac{dR_{on}{}^{L}}{dV_d} = \frac{1}{2\beta.(V_{gt} - V_d/2)^2} = \frac{\beta}{2}.R_{on}^{L\,2} \tag{8}$$

Note the proportionality of dR_{on}/dV_g and dR_{on}/dV_d with R_{on}^2.

B. Short channel MOSFET at strong inversion

For short channel devices, using the classical MOSFET model accounting for saturation velocity effect, we have [14]:

$$I_d = \frac{I_d{}^{L}}{1 + \frac{\mu_0 V_d}{v_{sat} L}} \tag{9}$$

where v_{sat} is the carrier saturation velocity. The associated expressions for the total on-resistance R_{on} ($R_{on}= V_d/I_d$) and associated derivatives dR_{on}/dV_g and dR_{on}/dV_d can also be derived and now read,

$$R_{on} = R_{on}{}^{L}.(1 + \frac{\mu_0 V_d}{v_{sat} L}) \tag{10}$$

$$\frac{dR_{on}}{dV_g} = \frac{dR_{on}{}^{L}}{dV_g}.(1 + \frac{\mu_0 V_d}{v_{sat} L}) = -\beta.R_{on}^{L\,2}.(1 + \frac{\mu_0 V_d}{v_{sat} L}) \tag{11}$$

$$\frac{dR_{on}}{dV_d} = \frac{\beta}{2}.R_{on}^{L\,2}.(1 + \frac{\mu_0 V_d}{v_{sat} L} + \frac{2\mu_0}{\beta.R_{on}^{L}.v_{sat} L}) \tag{12}$$

In this case, it should be noted that, unlike long channel devices, $(dR_{on}/dV_d)/(-dR_{on}/dV_g)$ is no longer constant with V_d.

3. Results and discussion

In order to validate the above analysis, the on-resistance $R_{on}(V_g,V_d)$ and the associated derivative characteristics have been reconstructed from $I_d(V_g,V_d)$ measurements performed on nMOSFETs from a 14nm FDSOI technology (as in [15] with gate width W=1µm and gate lengths from L=300nm down to L=60nm.

The impact of R_s and R_d was tested by adding external resistors (here R_{ext}=400Ω) in series with source and drain electrodes. For example, Fig. 1 illustrates how the $I_d(V_g)$ characteristics measured in linear operation (V_d=20mV) are significantly modified by the insertion of an external series resistance, especially as the gate length L is reduced. Figure 2 confirms the fact that the on-resistance R_{on} is well shifted by R_{ext} from linear to non linear triode region as V_d varies from 0 to 0.5V. Moreover, Fig. 3 clearly indicates that dR_{on}/dV_g is independent of R_{ext} for long and short channel devices. However, Fig. 4 reveals that, although dR_{on}/dV_d is independent of R_{ext} for long channel devices, it is slightly varying with R_{ext} for short devices. This fact could possibly be related to the assumptions we have considered. More precisely, in our theory low-field mobility, μ_0, is considered independent of the gate voltage, V_g, and also the source and drain series resistances, R_s and R_d, do not depend on V_g.

As a result, Fig. 5 shows that the generalized Y-function characteristics $Y_g(V_g)$ are well immune to R_{ext} as expected from Eqs (2)-(3) whatever the channel length. This feature demonstrates that the $Y_g(V_g)$ function does provide information on the intrinsic MOSFET operation – free from series resistance effect- not only in ohmic region but also in non linear operation region i.e. for large drain voltage. Instead, for short channel, the generalized Y-function characteristics $Y_d(V_d)$ of Fig. 6 slightly varies with R_{ext}, especially in triode region. Therefore, the $Y_d(V_d)$ characteristics are not perfectly immune to R_{ext}, contrary to $Y_g(V_g)$ characteristics.

Figure 7 shows that the ratio $(dR_{on}/dV_d)/(dR_{on}/dV_g)$ is lying around 0.5 from linear to non-linear region as predicted from Eqs (7)-(8) for long channel devices, emphasizing the consistency of R_{on} model of Eqs (6)-(8).

As suggested from Eq. (7) and shown in Fig. 8, the on-resistance R_{on} varies linearly with $(dR_{on}/dV_g)^{1/2}$ for long channel devices. This property could be used to extract the intrinsic R_{sd} of a single device after extrapolation of the straight line on y axis to zero abscissa as illustrated in Fig. 8. It should be noted that the extracted value of R_{sd} (≈650Ω) by this method falls in agreement with the one extracted with standard techniques using several gate lengths as in [15]. For short channel

devices, this property seems also to be applied as shown in Fig. 8, despite the difference in Eq. (11). However, in this case, the extracted R_{sd} value differs from the one extracted by standard techniques [15] and long channel case. Therefore, because of the extrapolation inaccuracy and limitation for short channel devices, we do not recommend this method for R_{sd} extraction on single short channel devices due to larger extrapolation error.

Figures 9 and 10 show the variations of $(dR_{on}/dV_d)/(dR_{on}/dV_g)$ with V_d for various channel lengths and how they can be satisfactorily modeled by saturation velocity effect using Eqs (11) and (12). However, the deviations at low drain voltage should be noted and are difficult to be interpreted by the simple model of Eqs (11) and (12).

In order to confirm the previous analysis and gain physical insight, we have performed calibrated modelling of the device characterstics using the Lambert function based compact model of [10] after inclusion of saturation velocity and series resistance effects. Typical calibration curves obtained with this compact model for the transfer characteristics $g_m(V_g)$ and output chacracteristics $I_d(V_d)$ are shown in Figs 11 and 12 for linear and non linear regions for short channel device (L=60nm). As can be seen from Fig. 13, the modeled $dR_{on}/dV_g(V_g)$ and $dR_{on}/dV_d(V_d)$ characteristics allow to reproduce satisfactorily the experimental data of Figs 3 and 4 and, in particular, some dependence of $dR_{on}/dV_d(V_d)$ curves with R_{ext}. These simulations confirm that $dR_{on}/dV_g(V_g)$ and, by turn, $Y_g(V_g)$ are perfectly immune to R_{ext}, whereas $dR_{on}/dV_d(V_d)$ and $Y_d(V_d)$ varies somehow with R_{ext}, expecially in short channel devices.

4. Conclusions

A new methodology for MOSFET characterization using the on-resistance $R_{on}(V_g,V_d)$ and associated derivatives dR_{on}/dV_g and dR_{on}/dV_d characteristics has been presented. This approach enables to eliminate the influence of R_{sd} not only in linear region but also in non-linear region of MOSFET operation. However, the $dR_{on}/dV_d(V_d)$ characteristics are not perfectly independent of external series resistance - especially for short devices, as confirmed by simulation. Instead, the

$dR_{on}/dV_g(V_g)$ and, by turn, $Y_g(V_g)$ characteristics are found perfectly immune to source-drain series resistance, generalizing the use of Y-function to non linear operation region. This methodology should be very useful for MOSFET intrinsic parameter extraction over full gate and drain voltage operation range.

Acknowledgments

This work has been partially supported by 3D-MUSE European project under Grant agreement n° 780548.

References

1. T. J. Krutsick, M. H. White, H.-S. Wong, and R. V. Booth, "An improved model of MOSFET modeling and parameter extraction", *IEEE Trans. Electron Devices*, 34, 1676-1680 (1987).
2. G. Ghibaudo, "New method for the extraction of MOSFET parameters", *IEE Electronic Letters*, 24, 543-545 (1988).
3. T. Taur, D. S. Zicherman, D. R. Lombardi, P. J. Restle, C. H. Hsu, H. I. Nanafi, M. R. Wordeman, B. Davari, and G. G. Shahidi, "A new 'shift and ratio' method for MOSFET channel-length extraction," *IEEE Electron Device Lett.*, 13, 267-269 (1992).
4. H. Katto, "Device parameter extraction in the linear region of MOSFET's," *IEEE Trans. Electron Devices*, 18, 408-410 (1997).
5. A. Ortiz-Conde, F. J. Garcia Sanchez, J. J. Liou, A. Cerdeira, M. Estrada, and Y. Yue, "A review of recent MOSFET threshold voltage extraction methods," *Microelectron. Reliab.*, 42, 583-596 (2002).
6. T. Tanaka, "Novel extraction method for size-dependent mobility based on BSIM3-like compact model, "*Japanese Journal of Applied Physics*, 44, 2424-2427 (2005).

7. D. Fleury, *A.* Cros, G. Bidal, J. Rosa and G. Ghibaudo, **"**A New Technique to Extract the Source/Drain Series Resistance of MOSFETs", IEEE Electron Device Letters, 30, 975-977 (2009).
8. D. Flandre, V. Kilchytska, and T. Rudenko, "g_m/I_d method for threshold voltage extraction applicable in advanced MOSFETs with nonlinear behavior above threshold," *IEEE Electron Device Lett.*, 31, 930-932 (2010).
9. F. Ferdousi, R. Rios, K. J. Kuhn, "Improved MOSFET characterization technique for single channel length, scaled transistors", Solid State Electronics, 104, 44-46 (2015).
10. T.A. Karatsori, C.G. Theodorou, E.G. Ioannidis, S. Haendler, E. Josse, C.A. Dimitriadis, G. Ghibaudo, "Full gate voltage range Lambert-function based methodology for FDSOI MOSFET parameter extraction", *Solid-State Electronics*, 111, 123–128 (2015).
11. J.B. Henry, Q. Rafhay, A. Cros, and G. Ghibaudo, "New Y-function based MOSFET parameter extraction method from weak to strong inversion range", Solid State Electronics, 123, 84-88 (2016).
12. B. Cretu, T. Boutchacha, G. Ghibaudo and F. Balestra, "New ratio method for effective channel length and threshold voltage extraction in MOS transistors", IEE Electronics Letters, 37, 717-719 (2001).
13. Y. Xu, T. Minari, K. Tsukagoshi, R. Gwoziecki, R. Coppard, F. Balestra and G. Ghibaudo, "Power transfer-length method for full biasing contact resistance evaluation of organic field-effect transistors", Organic Electronics, 12 , 2019-2024 (2011).
14. Y. Taur and T. King, "Fundamentals of modern VLSI", Chap. 3 "MOSFET devices", p. 188 (Cambridge, 1998).
15. T. A. Karatsori, C. G. Theodorou, E. Josse, C. A. Dimitriadis, , and G. Ghibaudo**, "**All operation region characterization and modeling of drain and gate current mismatch in 14nm Fully Depleted SOI MOSFETs", IEEE Trans. Electron Devices, 64, 2080-2085 (2017).

Figure captions

Fig. 1. Experimental $I_d(V_g)$ characteristics with R_{ext}=400Ω (dashed line) and without R_{ext} (solid line) for V_d=20mV and various channels L.

Fig. 2. $R_{on}(V_d)$ with R_{ext}=400Ω (dashed line) and without R_{ext} (solid line) for V_g=1V (L=60nm and 300nm, Vt=0.4V).

Fig. 3. $dR_{on}/dV_g(V_d)$ with R_{ext}=400Ω (dashed line) and without R_{ext} (solid line) for V_g=1V (L=300nm and 60nm).

Fig. 4. $dR_{on}/dV_d(V_d)$ with R_{ext}=400Ω (dashed line) and without R_{ext} (solid line) for V_g=1V (L=300nm and 60nm).

Fig. 5. $Y_g(V_g)$ with R_{ext}=400Ω (dashed line) and without R_{ext} (solid line) for various V_d and V_g=1V (L=60nm and 300nm).

Fig. 6. Y_d vs $\sqrt{V_d}$ with R_{ext}=400Ω (dashed line) and without R_{ext} (solid line) for V_g=1V (L=60nm and 300nm).

Fig. 7. $(dR_{on}/dV_d)/(dR_{on}/dV_g)$ vs V_d with R_{ext}=400Ω (dashed line) and without R_{ext} (solid line) for V_g=1V (L=300nm).

Fig. 8. R_{on} vs $(dR_{on}/dV_g)^{1/2}$ as V_d is varying from 0 to 0.5V with R_{ext}=400Ω (dashed line) and without R_{ext} (solid line) for V_g=1V (L=60nm and 300nm). Extraction of R_{sd} by extrapolation on y axis to zero abscissa.

Fig. 9. Experimental $(dR_{on}/dV_d)/(dR_{on}/dV_g)$ vs V_d without R_{ext} for various L (V_g=1V).

Fig. 10. Modeled $(dR_{on}/dV_d)/(dR_{on}/dV_g)$ vs V_d for various L (V_g=1V, v_{sat}=2.10^7cm/s, μ_0=140cm^2/Vs, V_t=0.4V).

Fig. 11. Experimental (left) and modeled (right) $g_m(V_g)$ characteristics with R_{ext}=400Ω and without R_{ext} for L=60nm (V_d=20mV).

Fig. 12. Experimental (left) and modeled (right) $I_d(V_d)$ characteristics with R_{ext}=400Ω and without R_{ext} for L=60nm (V_g=1V).

Fig. 13. Modeled dR_{on}/dV_g and dR_{on}/dV_d vs V_d characteristics with R_{ext}=400Ω and without R_{ext} for L=60nm (V_g=1V).

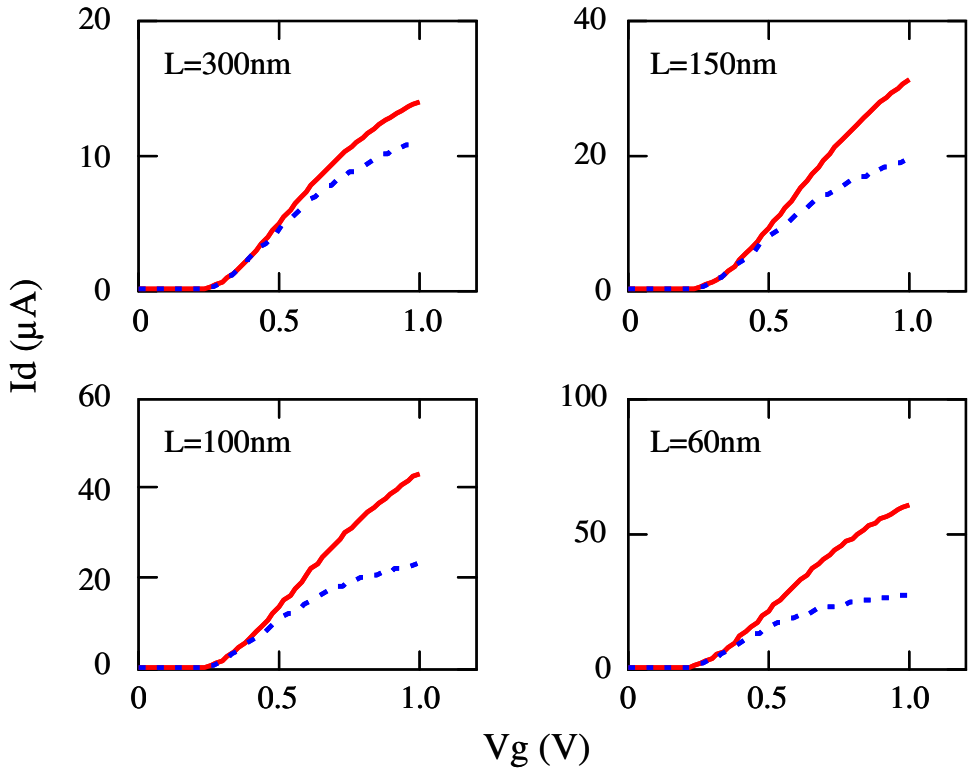

Fig. 1. Experimental $I_d(V_g)$ characteristics with R_{ext}=400Ω (dashed line) and without R_{ext} (solid line) for V_d=20mV and various channels L.

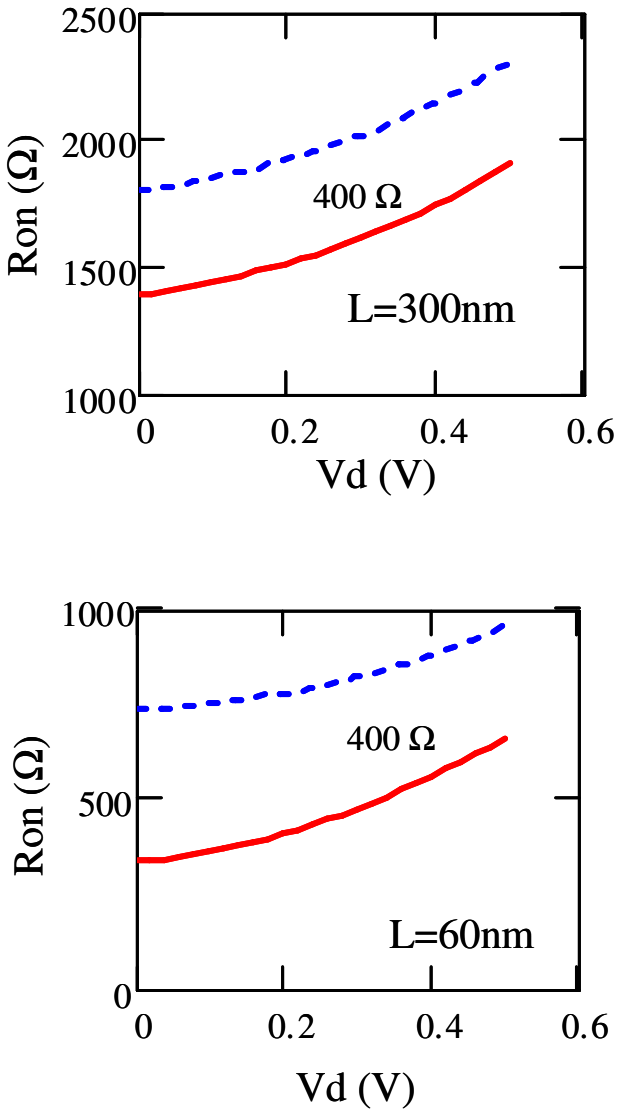

Fig. 2. $R_{on}(V_d)$ with R_{ext}=400Ω (dashed line) and without R_{ext} (solid line) for V_g=1V (L=60nm and 300nm, Vt=0.4V).

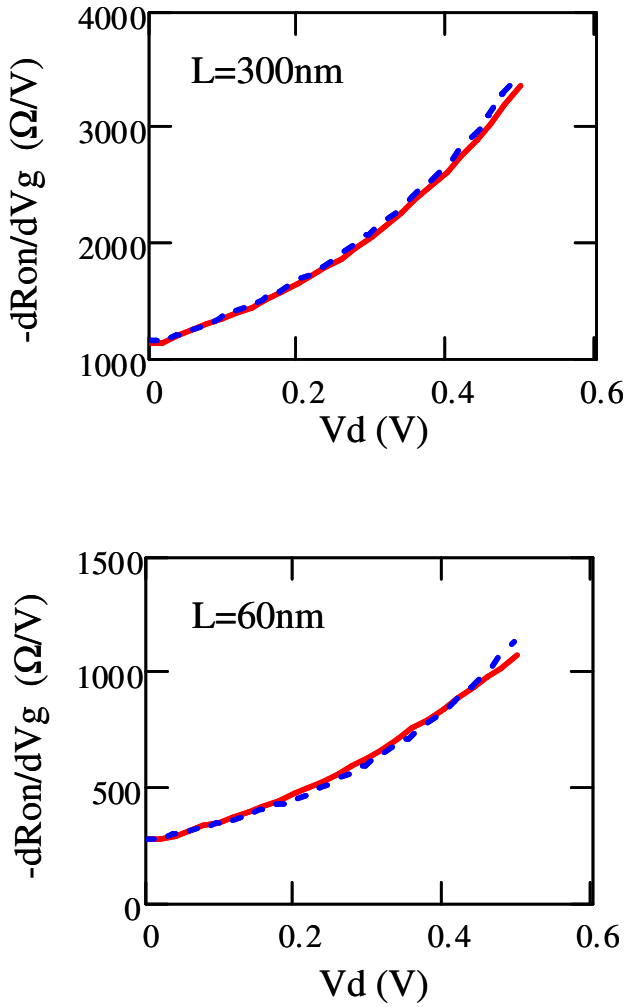

Fig. 3. $dR_{on}/dV_g(V_d)$ with R_{ext}=400Ω (dashed line) and without R_{ext} (solid line) for V_g=1V (L=300nm and 60nm).

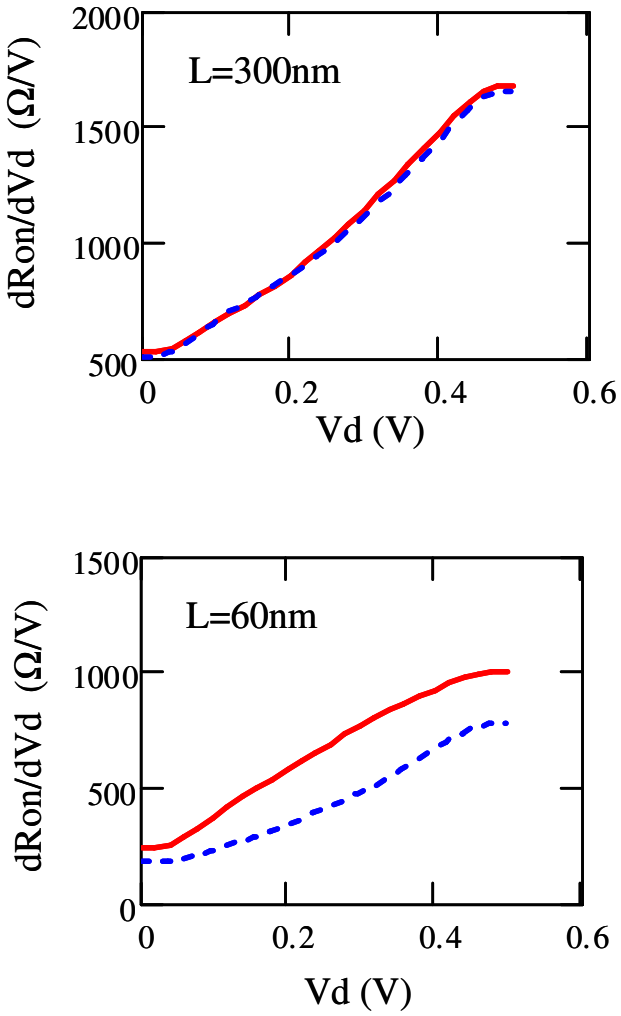

Fig. 4. $dR_{on}/dV_d(V_d)$ with R_{ext}=400Ω (dashed line) and without R_{ext} (solid line) for V_g=1V (L=300nm and 60nm).

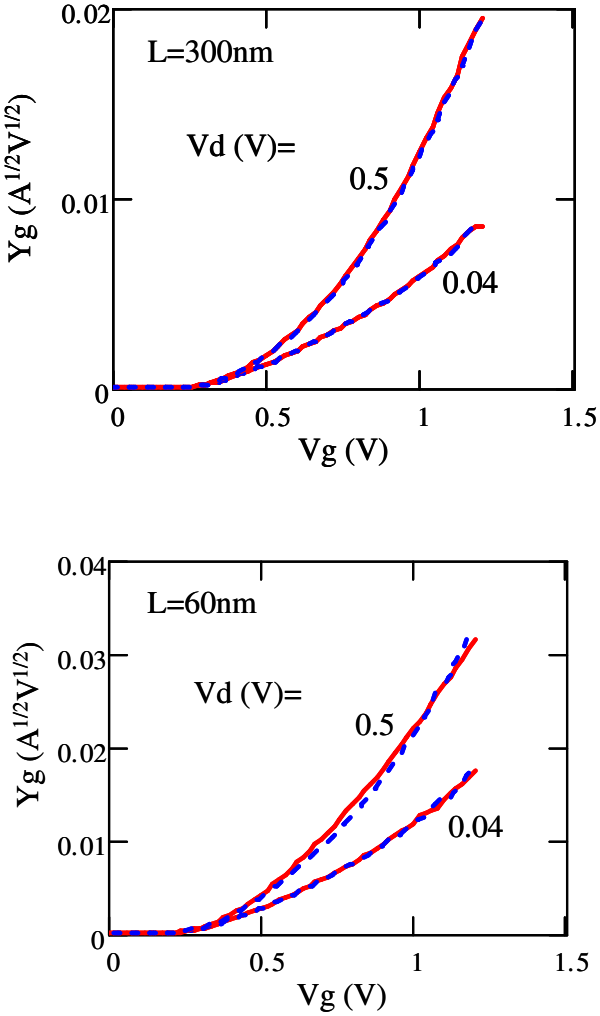

Fig. 5. $Y_g(V_g)$ with R_{ext}=400Ω (dashed line) and without R_{ext} (solid line) for various V_d and V_g=1V (L=60nm and 300nm).

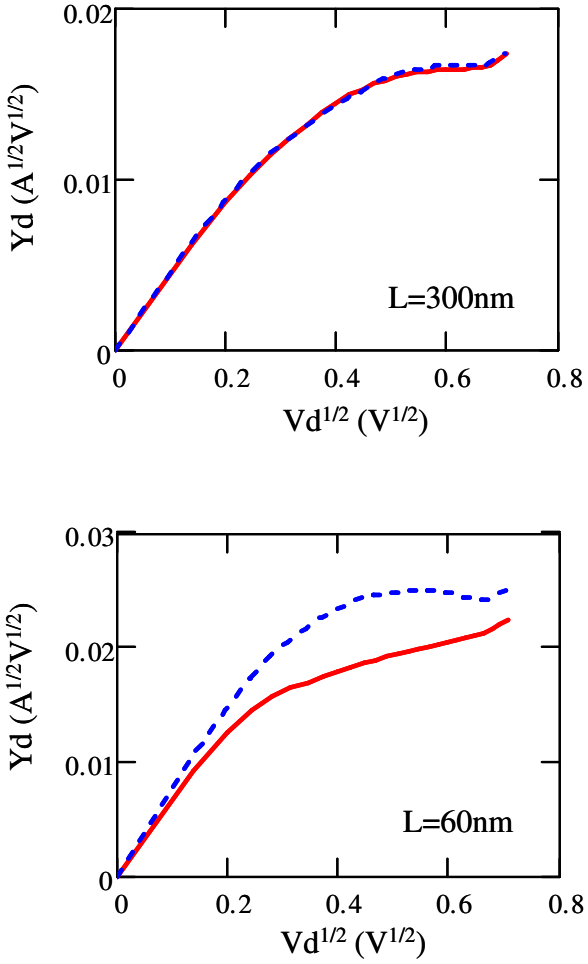

Fig. 6. Y_d vs $\sqrt{V_d}$ with R_{ext}=400Ω (dashed line) and without R_{ext} (solid line) for V_g=1V (L=60nm and 300nm).

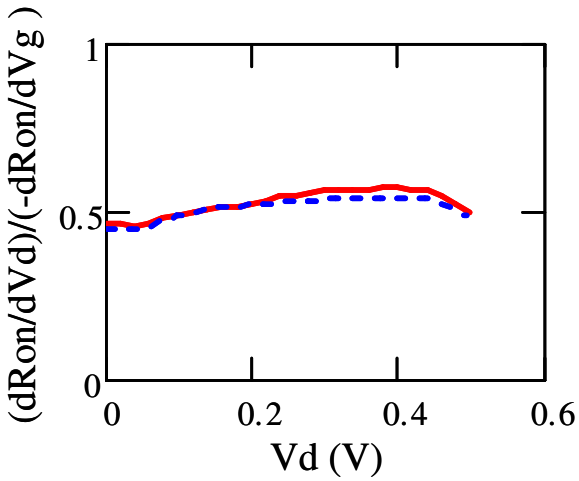

Fig. 7. $(dR_{on}/dV_d)/(dR_{on}/dV_g)$ vs V_d with R_{ext}=400Ω (dashed line) and without R_{ext} (solid line) for V_g=1V (L=300nm).

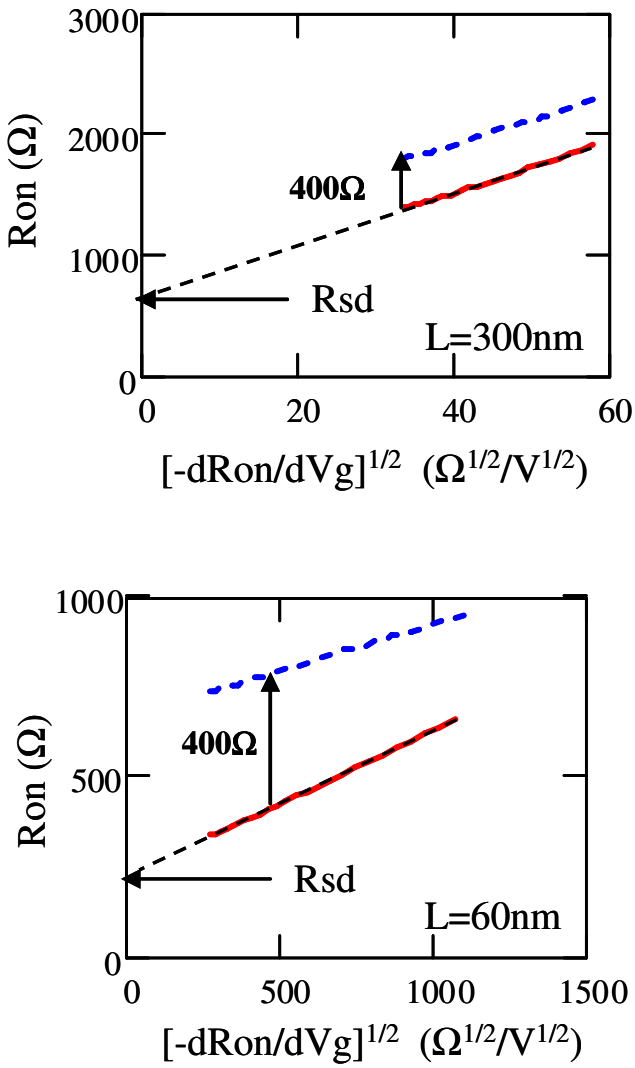

Fig. 8. R_{on} vs $(dR_{on}/dV_g)^{1/2}$ as V_d is varying from 0 to 0.5V with R_{ext}=400Ω (dashed line) and without R_{ext} (solid line) for V_g=1V (L=60nm and 300nm). Extraction of R_{sd} by extrapolation on y axis to zero abscissa.

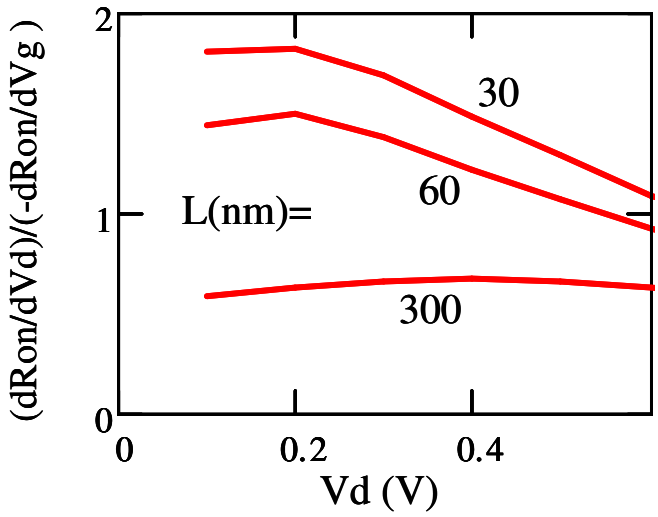

Fig. 9. Experimental (dR_{on}/dV_d)/(dR_{on}/dV_g) vs V_d without R_{ext} for various L (V_g=1V).

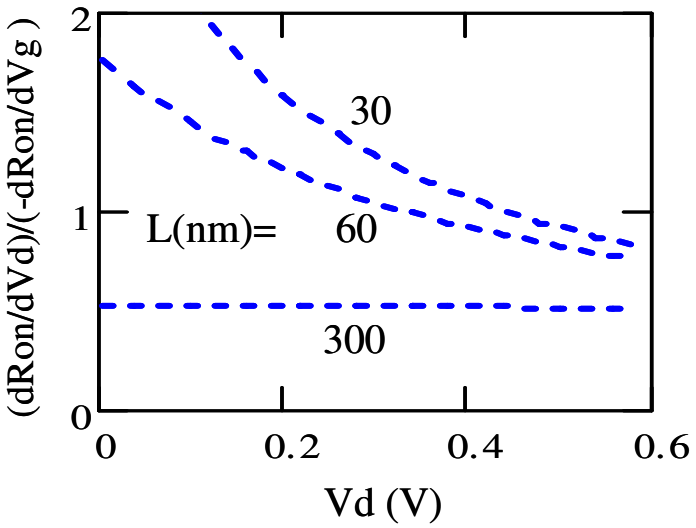

Fig. 10. Modeled $(dR_{on}/dV_d)/(dR_{on}/dV_g)$ vs V_d for various L (V_g=1V, v_{sat}=2.10^{7}cm/s, μ_0=140cm^2/Vs, V_t=0.4V).

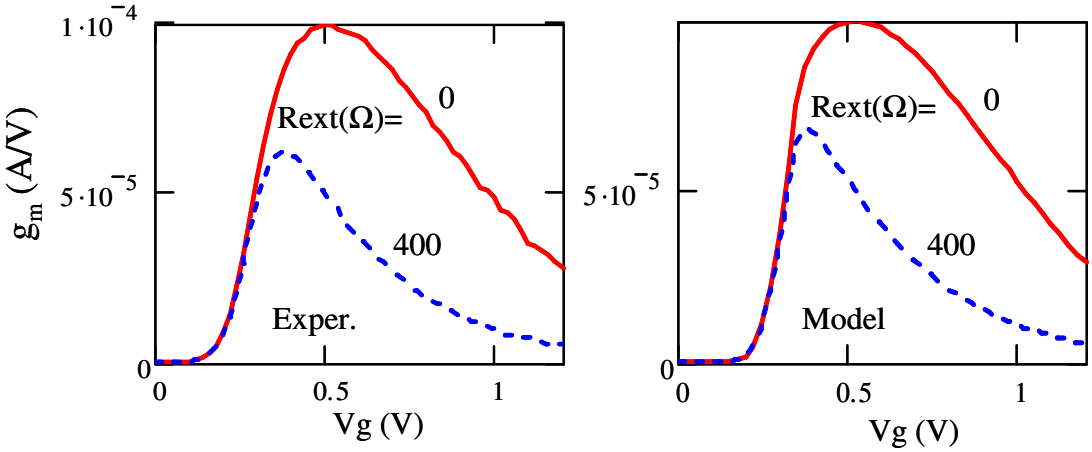

Fig. 11. Experimental (left) and modeled (right) $g_m(V_g)$ characteristics with R_{ext}=400Ω and without R_{ext} for L=60nm (V_d=20mV).

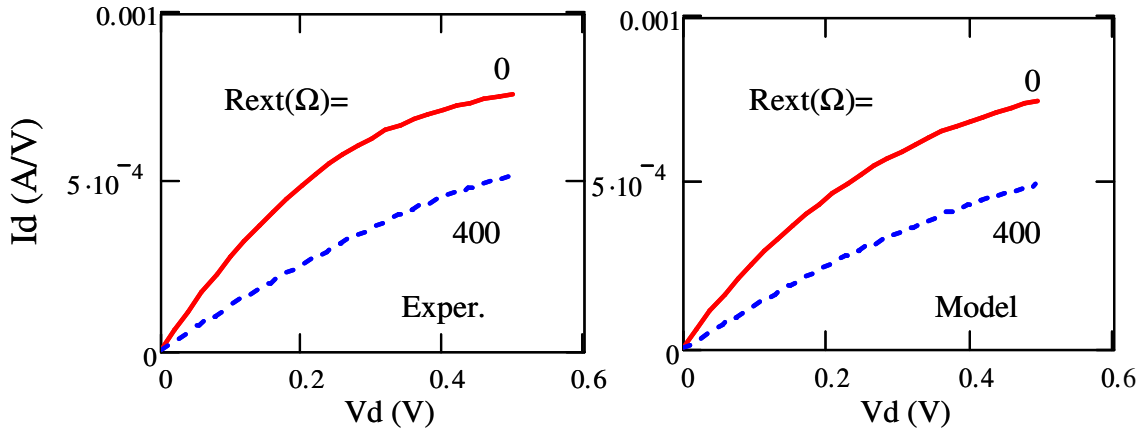

Fig. 12. Experimental (left) and modeled (right) $I_d(V_d)$ characteristics with R_{ext}=400Ω and without R_{ext} for L=60nm (V_g=1V).

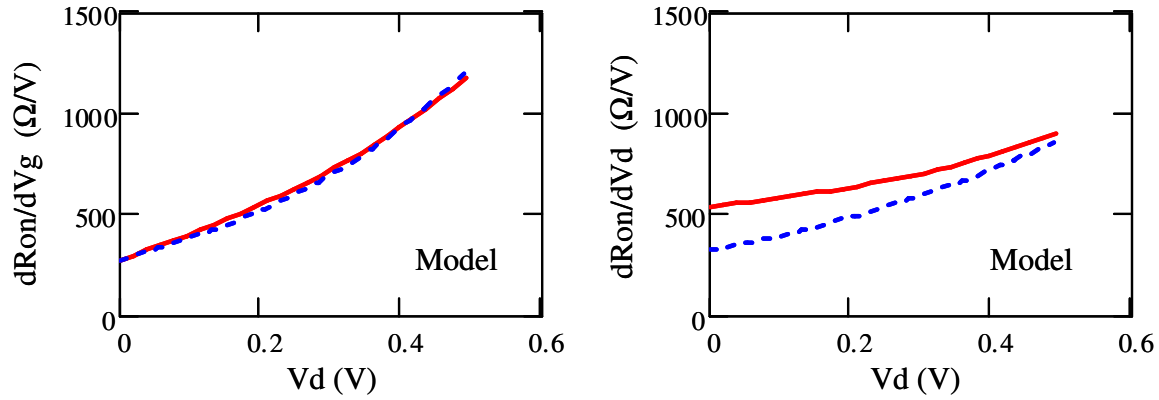

Fig. 13. Modeled dR_{on}/dV_g and dR_{on}/dV_d vs V_d characteristics with R_{ext}=400Ω and without R_{ext} for L=60nm (V_g=1V).